Euro. Jnl of Applied Mathematics (2001), *vol.* 12, *pp.* 357–366. Printed in the United Kingdom

Damped waves generated by a moving pressure distribution

J.-M. VANDEN-BROECK

School of Mathematics, The University of East Anglia, Norwich NR4 7TJ, UK

(*Received 22 September 1999; revised 6 March 2001*)

Free surface flows generated by a moving distribution of pressure are considered. The fluid consists of two superposed layers in a two-dimensional channel. The upper layer is inviscid and the lower layer, which is introduced as a damping mechanism, is modelled by the mathematically convenient lubrication equations. Numerical and analytical solutions are presented. Special attention is given to solutions for which there is a train of waves on each side of the distribution of pressure. It is shown that, depending on the values of the parameters, the short waves can appear on either side of the distribution of pressure.

1 Introduction

There is a vast literature on potential free surface flows where the fluid is assumed to be bounded below by a rigid horizontal bottom. Although this is usually a very good assumption, there are practical situations in which it is not justified. For example the bottom of a channel might be covered by a layer of mud or grease. Here we investigate an idealised problem where the rigid bottom is replaced by a layer with a damping mechanism. Our aim is to model damping while keeping the mathematics simple. Therefore, we do not use the Navier Stokes equations in the lower layer. Instead, we use a mathematical device which might not be physically realisable, but which allows the reformulation of the problem as a nonlinear integro-differential equation. We shall refer to the lower layer as the 'dissipative layer'. The calculations presented generalise the work of Vanden-Broeck & Miloh [9] by including the effect of the surface tension T at the interface between the dissipative layer and the potential flow. As we shall see, the properties of the flows with a dissipative layer differ from those with a rigid bottom.

Our configuration consists of two superposed layers of fluid in a channel (see Figure 1). The lower layer is dissipative. The upper layer is inviscid and bounded above by a free surface. Both fluids are incompressible and the flow in the upper layer is irrotational. The flow is generated by a disturbance moving at a constant velocity C to the left. The disturbance can be an insect, a ship or a submerged object. The qualitative properties of the solutions presented here are independent of the particular form of the disturbance. Here we assume that the disturbance is a distribution of pressure with a compact support.

We assume that the flow is two-dimensional, and we take a frame of reference moving with the pressure distribution. There are then both steady and unsteady solutions [4]. Here we restrict our attention to steady solutions.

https://doi.org/10.1017/S095679250100451X Published online by Cambridge University Press

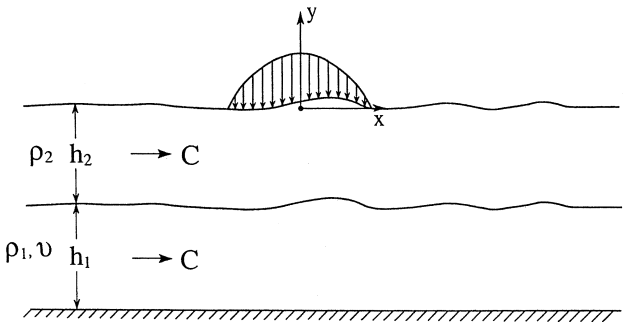

FIGURE 1. Sketch of the flow and coordinates.

The corresponding problem with a rigid horizontal bottom (i.e. the configuration of Figure 1 where the thickness of the dissipative layer is zero) was considered by Rayleigh [6] (see also Lamb [2]), who assumed that the magnitude of the pressure distribution is small. The equations are then linearised and the problem solved by Fourier transforms. The properties of the linear solution can be understood by looking at the most general form of the solution in the far field (i.e. as $x \to \pm\infty$). If the most general form is a flat free surface, then the solution of the linear problem is unique. On the other hand, if the most general form is a train of periodic waves, then the solution of the linear problem is not unique. It is then necessary to supply a radiation condition to fix uniquely the linear solution. One way to impose the radiation condition is to solve a problem with an artificial viscosity (the Rayleigh viscosity), and then take the limit as the artificial viscosity approaches zero [6, 2]. Another way is to use Ruvinsky *et al.*'s [7] approach to model a viscous flow, and then take the limit as the viscosity approaches zero [5]. As we shall see, a third way is to solve the problem with a dissipative lower layer, and then take the limit as its thickness approaches zero.

We solve the flow configuration of Figure 1 numerically. Our solutions are nonlinear, and no assumptions are made on the magnitude of the distribution of pressure. However, we approximate the flow in the lower layer by using the lubrication equations, instead of the Navier Stokes equations, even when the thickness of the lower layer is not small. Therefore, the lubrication approximation should be viewed in this paper as a convenient mathematical device to simulate dissipation. This device enables us to formulate the problem as an inviscid flow with appropriate boundary conditions, which is then reformulated as a boundary integral equation. This equation is discretized, and the resultant algebraic equations are solved by Newton's method. The numerical procedure is similar to that used by many investigators to study purely inviscid free surface flows (see, for example, Vanden-Broeck & Tuck [10], Forbes & Schwartz [1] and Vanden-Broeck & Dias [8]). It reduces to the scheme used by Vanden-Broeck & Miloh [9] when $T = 0$.

The formulation and the numerical procedure are summarised in §2. The reader is referred to Vanden-Broeck & Miloh [9] for further details. The results are presented in § 3.

2 Mathematical formulation

We consider a flow with two layers bounded below by a horizontal bottom and above by a free surface (see Figure 1). The lower layer is an incompressible and 'dissipative'

https://doi.org/10.1017/S095679250100451X Published online by Cambridge University Press

fluid of density ρ_1. The upper layer is an incompressible and inviscid fluid of density ρ_2. A pressure distribution moving to the left at a constant velocity C is acting on the free surface. We take a frame of reference moving with the pressure distribution and we seek steady solutions.

We define cartesian coordinates with the x-axis along the level of the free surface far upstream and the y-axis directed vertically upwards. Gravity is acting along the negative y-axis. We describe the shape of the free surface by $y = \eta_F(x)$ and the shape of the interface between the two layers by $y = \eta_I(x)$. The functions $\eta_F(x)$ and $\eta_I(x)$ have to be found as part of the solution.

As $x \to \pm\infty$, the lower and upper layers are characterized by constant thickness h_1 and h_2 and a constant velocity C. The flow in the upper layer is irrotational. In the lower layer, we use the lubrication equations instead of the Navier Stokes equations. Thus, we write

$$u_x + v_y = 0$$

$$0 = -\frac{1}{\rho_1} p_x + \nu u_{yy}$$

$$0 = -\frac{1}{\rho_1} p_y - g. \tag{1}$$

Here u and v are the x and y components of the velocity, and ν is the viscosity. We emphasize that we use the lubrication equations (1), even when the lower layer is not thin. This mathematical device enables us to solve the problem by a boundary integral equation method. We refer to ν as the viscosity for convenience, although we are not solving the full Navier Stokes equations and the lower layer might be too thick for the lubrication approximation to apply. In the upper layer the flow is irrotational. Therefore, the complex velocity $u - C - iv$ is an analytic function of $z = x + iy$ in the strip $\eta_I(x) < y < \eta_F(x)$.

The equations are to be solved subject to the boundary conditions

(i) $u = C, v = 0$ on $y = -h_1 - h_2$,
(ii) $u_y = 0$ on $y = \eta_I^-(x)$,
(iii) $p(x, \eta_I^-(x)) = p(x, \eta_I^+(x)) + T \frac{\eta_{Ixx}}{(1+\eta_{Ix}^2)^{3/2}}$
(iv) $v = u\eta_{Ix}$ on $y = \eta_I^{\pm}(x)$,
(v) $v = u\eta_{Fx}$ on $y = \eta_F(x)$,
(vi) $\frac{(u^2+v^2)}{2} + g\eta_F(x) + \frac{P_A(x)}{\rho_2} = \frac{C^2}{2}$ on $y = \eta_F(x)$
(vii) $u \to C, \quad v \to 0$ as $|x| \to \infty$.

Here T is the surface tension and η_I^- and η_I^+ denote the lower and upper sides of the interface η_I. The conditions (ii), (iii), (iv) on the interface $y = \eta_I(x)$ represent respectively continuity of tangential stress, the pressure jump due to surface tension and the kinematic conditions. The conditions (v) and (vi) on the free surface $y = \eta_F(x)$ are the kinematic condition and the dynamic boundary condition. The function $P_A(x)$ in (vi) is the prescribed distribution of pressure. We assume that $P_A(x)$ has compact support, i.e. that $P_A(x)$ vanish outside some finite interval. The condition (vii) requires that the waves decay in the far field.

The problem can then reformulated as a system of integro differential equations by following the derivation of sections 2 and 3 of Vanden-Broeck & Miloh [9]. Using

https://doi.org/10.1017/S095679250100451X Published online by Cambridge University Press

dimensionless variables with C as the unit velocity and h_2 as the unit length, we obtain the following system:

$$\pi[u_F(x)-1] =$$
$$-\int_{-\infty}^{+\infty}\frac{[u_F(s)-1+v_F(s)\eta_F'(s)][\eta_F(x)-\eta_F(s)]+[(u_F(s)-1)\eta_F'(s)-v_F(s)](s-x)}{(s-x)^2+(\eta_F(s)-\eta_F(x))^2}\,ds$$
$$+\int_{-\infty}^{+\infty}\frac{[u_I^+(s)-1+v_I^+(s)\eta_I'(s)][\eta_F(x)-\eta_I(s)]+[(u_I^+(s)-1)\eta_I'(s)-v_I^+(s)](s-x)}{(s-x)^2+(\eta_I(s)-\eta_F(x))^2}\,ds \tag{2}$$

$$\pi[u_I^+(x)-1] =$$
$$-\int_{-\infty}^{+\infty}\frac{[u_F(s)-1+v_F(s)\eta_F'(s)][\eta_I(x)-\eta_F(s)]+[(u_F(s)-1)\eta_F'(s)-v_F(s)](s-x)}{(s-x)^2+(\eta_F(s)-\eta_I(x))^2}\,ds$$
$$+\int_{-\infty}^{+\infty}\frac{[u_I^+(s)-1+v_I^+(s)\eta_I'(s)][\eta_I(x)-\eta_I(s)]+[(u_I^+(s)-1)\eta_I'(s)-v_I^+(s)](s-x)}{(s-x)^2+(\eta_I(s)-\eta_I(x))^2}\,ds \tag{3}$$

$$\frac{\delta-1}{F^2}\eta_I'(x)+\frac{3}{R}\frac{\eta_I(x)+1}{(\eta_I(x)+\beta+1)^3}+\delta(uu_x+vv_x)+\kappa\frac{d}{dx}\frac{\eta_{Ixx}}{(1+\eta_{Ix}^2)^{3/2}}=0, \tag{4}$$

$$v_I^+(x)=u_I^+(x)\eta_I'(x), \tag{5}$$

$$u_F^2(x)+v_F^2(x)+\frac{2}{F^2}\eta_F(x)+2P_A(x)=1. \tag{6}$$

The parameters in (2)–(6) are the Froude number

$$F=\frac{C}{(gh_2)^{1/2}}, \tag{7}$$

the Reynolds number

$$R=\frac{Ch_2}{\nu}, \tag{8}$$

the depth ratio

$$\beta=\frac{h_1}{h_2}, \tag{9}$$

the capillary number

$$\kappa=\frac{T}{\rho C^2h_2}, \tag{10}$$

and the density ratio

$$\delta=\frac{\rho_1}{\rho_2}. \tag{11}$$

Equations (2) and (3) follow from applying Cauchy integral formula to the analytic function $u-iv-1$ with a contour consisting of $y=\eta_F(x)$, $y=\eta_I(x)$ and two vertical lines at $|x|=\infty$. Relations (4)–(6) follow from (*i*)–(*vii*). For given values of F, R, β, κ and δ, (2)–(6) define a system of integro-differential equations for the four unknown functions $u_F(x)$, $\eta_F'(x)$, $u_I^+(x)$ and $\eta_I'(x)$. This system is solved numerically by using the scheme described in section 4 of Vanden-Broeck & Miloh [9]. The main difference is that the second derivative of η_I needs to be evaluated (see (4)). This is done by central differences. In all the calculations we chose

$$P_A(x)=0, \quad \text{for} \quad |x|>b$$

https://doi.org/10.1017/S095679250100451X Published online by Cambridge University Press

and

$$P_A(x) = \frac{\epsilon}{2} \exp \frac{25b^2}{x^2 - 25b^2} \quad \text{for} \quad |x| < b. \tag{12}$$

Here ϵ and b are two constants which define the strength and the length of the pressure distribution. We note here a typographical error in Vanden-Broeck & Miloh [9]. Formula (3.13) of Vanden-Broeck & Miloh [9] should be replaced by formula (12) of this paper.

3 Discussion of results

The numerical results show that for $0 < R < \infty$, the waves (if present) are of decaying amplitude as $x \to \pm\infty$. For $R = 0$ and $R = \infty$, the waves (if any) are of constant amplitude as $x \to \pm\infty$. This constant amplitude is usually small when ϵ is small. These two facts suggest that some useful insight into the problem can be gained by linearising the equations around a flat free surface (i.e. a uniform stream) and seeking wavelike solutions. This will lead to useful expressions for the asymptotic behaviours of the flow as $x \to \pm\infty$.

Therefore, we write $u = 1 + u^*$, $v = v^*$, $\eta_F = \eta_F{}^*$, $\eta_I = -1 + \eta_I{}^*$, where the variables with $*$ denote small perturbations.

For simplicity of the formulas and presentation, we assume in the remaining part of the paper $\delta = 1$. Retaining only the terms linear in u^*, v^*, $\eta_I{}^*$ and $\eta_F{}^*$ yields after some algebra

$$\frac{3}{R\beta^3} v^* + u^*_{xx} + \kappa v^*_{xxx} = 0 \quad y = -1, \tag{13}$$

$$u^*_x + \frac{1}{F^2} v^* = 0 \quad y = 0. \tag{14}$$

Since the flow is irrotational in the upper layer, we can define a potential function ϕ^* such that

$$u^* = \phi^*_x, \quad v^* = \phi^*_y. \tag{15}$$

We seek wavelike solutions of the form

$$\phi^* = e^{ikx}[Ae^{ky} + Be^{-ky}]. \tag{16}$$

Here A, B and k are constants. When the constant k is real, the wave is of constant amplitude and can occur both for $x > 0$ and $x < 0$. When k is complex, we write $k = k_r + ik_i$ and refer to k_r as the wavenumber and k_i as the rate of decay. Since we require bounded solutions and

$$e^{ikx} = e^{-k_i x} e^{ik_r x}, \tag{17}$$

(16) implies that waves with $k_i > 0$ occur for $x > 0$ and waves with $k_i < 0$ occur for $x < 0$.

To evaluate k, we substitute (15) and (16) into (13) and (14), and obtain the following linear system for A and B:

$$\left[\frac{3}{R\beta^3} e^{-k} - ik^2 e^{-k} - \kappa ik^3 e^{-k}\right] A + \left[-\frac{3}{R\beta^3} e^{k} - ik^2 e^{k} + \kappa ik^3 e^{k}\right] B = 0 \tag{18}$$

$$\left[-k + \frac{1}{F^2}\right] A - \left[k + \frac{1}{F^2}\right] B = 0 \tag{19}$$

https://doi.org/10.1017/S095679250100451X Published online by Cambridge University Press

Equations (18) and (19) have a nontrivial solution for A and B, if the determinant of the coefficients vanishes. Therefore, we require

$$e^{-k}\Big[-\frac{3}{R\beta^3}(k+\frac{1}{F^2})+ik^3+\frac{ik^2}{F^2}+\kappa i(k^4+\frac{k^3}{F^2})\Big]-e^{k}\Big[\frac{3}{R\beta^3}(k-\frac{1}{F^2})$$

$$+ik^3-\frac{ik^2}{F^2}+\kappa i(-k^4+\frac{k^3}{F^2})\Big]=0 \tag{20}$$

We note that (20) reduces to

$$F^2=\frac{\tanh k}{k} \tag{21}$$

for $R=0$ and to

$$F^2=\frac{1-\kappa k\tanh k}{k\tanh k-\kappa k^2} \tag{22}$$

for $R=\infty$. The problem with $R=\infty$ is completely inviscid and corresponds to a lower layer in which the pressure is hydrostatic. When $R=0$, the surface of the dissipative layer is flat and the classical configuration with a rigid bottom is recovered.

We now use the results (20)–(22) to discuss the results obtained by the numerical scheme outlined in § 2. Typical profiles of the free surface and of the surface of the dissipative layer are shown in Figures 2 and 3. For $0<R<\infty$, there are in general trains of waves both in front and at the back of the distribution of pressure. These trains are more visible on the surface of the dissipative layer than on the free surface and are of decaying amplitude as $|x|\to\infty$ (see Figures 2 and 3). We denote by k^{front} and k^{back} the values of k associated with these two train of waves. Here 'front' and 'back' refer to the regions $x<0$ and $x>0$ of Figure 1. Since the waves are of decaying amplitudes, the values of k^{front} and k^{back} can be evaluated from the linear theory (i.e. from (20)). For the flow of Figure 2, we set $F=0.89$, $\kappa=0.4$, $R=60$, $\beta=0.25$ and solve (20) for k by Newton's method. This yields two roots $k=2.94-0.78i$ and $k=1.07+0.42i$. Requiring the waves to decay at infinity (i.e. using (17)), we obtain $k^{front}=2.94-0.78i$ and $k^{back}=1.07+0.42i$. Next we consider the flow of Figure 3. We set $F=0.55$, $\kappa=0.4$, $R=60$ and $\beta=0.25$ and obtain in the same way $k^{front}=2.99-0.73i$ and $k^{back}=3.30+0.03i$.

We note that that $k_r^{front}>k_r^{back}$ in Figure 2 whereas $k_r^{front}<k_r^{back}$ in Figure 3. In other words, the waves of shorter wavelength are at the front of the distribution of pressure in Figure 2 and at the back in Figure 3.

To understand better this difference between the solutions of Figure 2 and 3, we consider the limiting case $R=\infty$. Then we can no longer determine which train of waves will appear in front or at the back of the distribution of pressure from the sign of k_i since $k_i=0$ when $R=\infty$. The solution of of the linearised version of the flow of Figure 1 is then non-unique. However the physically relevant solution can be recovered by imposing an extra 'radiation condition'. This condition requires that no wave energy is being generated at 'infinity' [3]. Since the energy travels with the group velocity, this condition implies that waves for which the group velocity is larger than the phase velocity are at the front of the disturbance and those for which the group velocity is smaller than the phase velocity are at the back of the disturbance. Here the phase velocity is U and the group velocity is

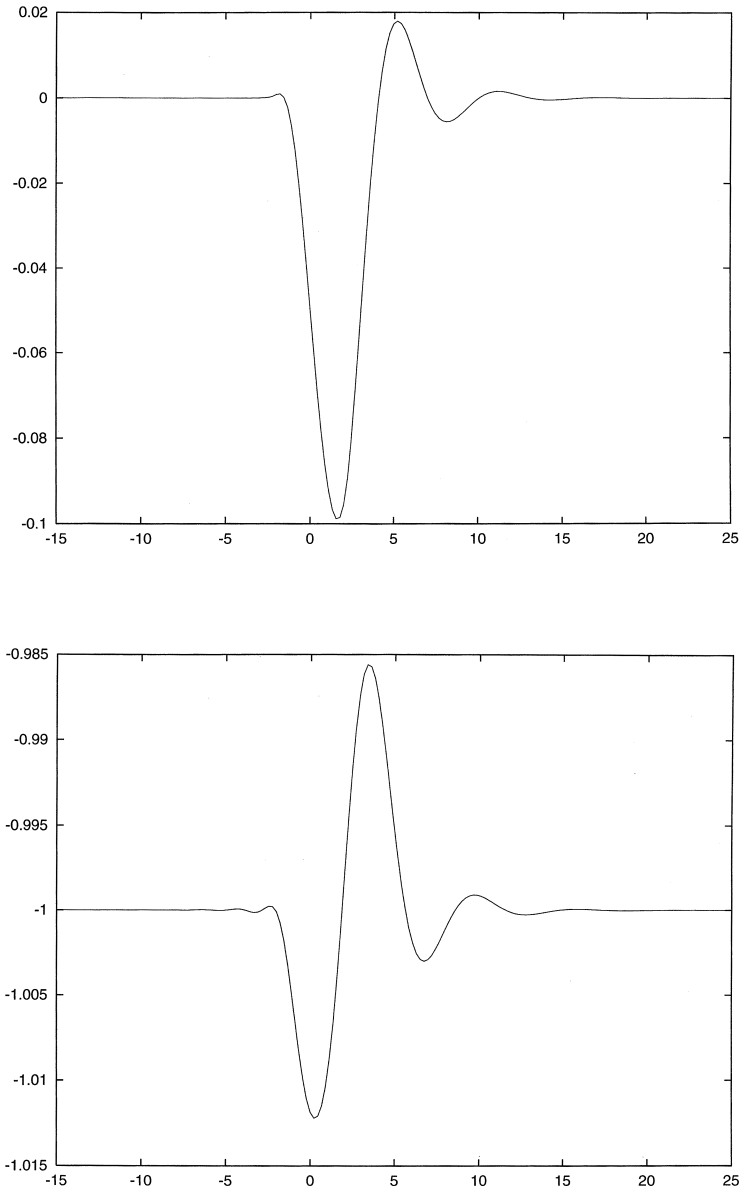

FIGURE 2. Free surface profile (a) and profile of the surface of the dissipative layer (b) for $F = 0.89$, $b = 0.5$, $\delta = 1$, $\beta = 0.25$, $\epsilon = 0.5$, $\kappa = 0.4$ and $R = 60$.

defined as

$$C_g = \frac{d\Omega}{dK} \tag{23}$$

where $\Omega = KC$ is the angular frequency and K the wavenumber. Using our dimensionless variables and (7), we rewrite (23) as

$$c_g = 1 + \frac{k}{F}\frac{dF}{dk} \tag{24}$$

https://doi.org/10.1017/S095679250100451X Published online by Cambridge University Press

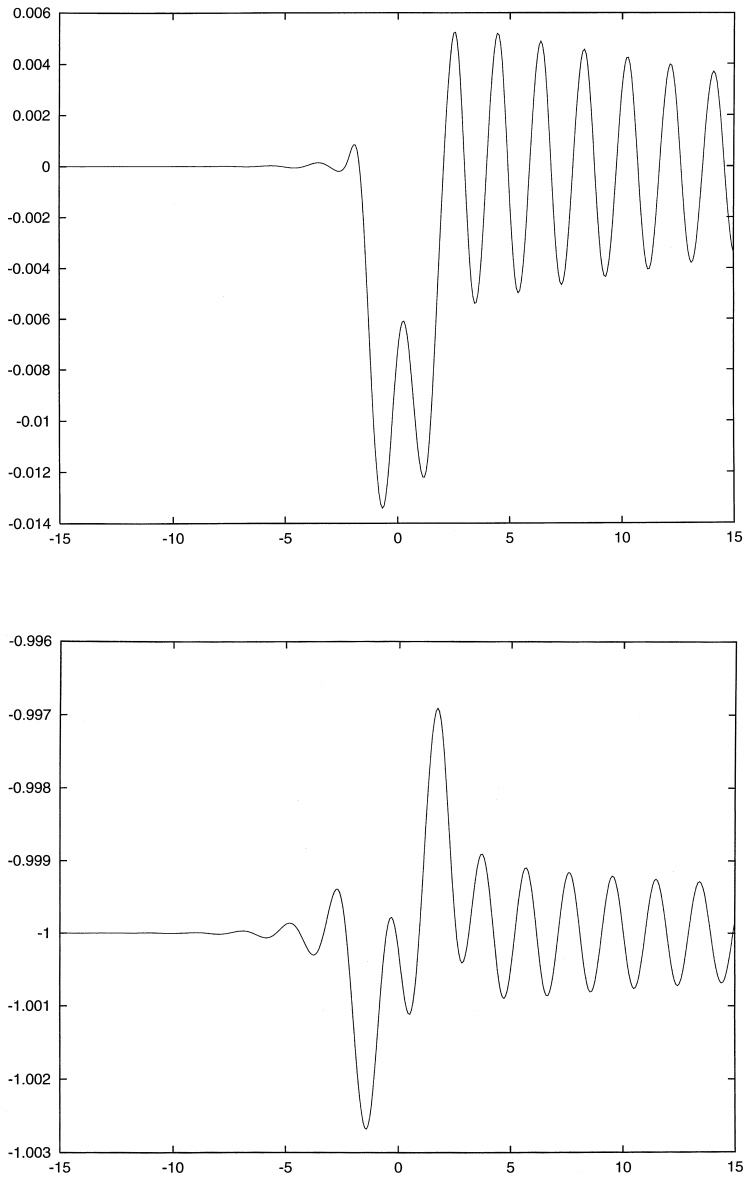

FIGURE 3. Same as Figure 2 with $F = 0.55$.

where c_g is the dimensionless group velocity. The dimensionless phase velocity is 1. It follows that

$$c_g > 1 \quad \text{when} \quad \frac{dF}{dk} > 0 \tag{25}$$

and

$$c_g < 1 \quad \text{when} \quad \frac{dF}{dk} < 0. \tag{26}$$

Waves satisfying (25) appear at the front of the disturbance and those satisfying (26) at the back.

https://doi.org/10.1017/S095679250100451X Published online by Cambridge University Press

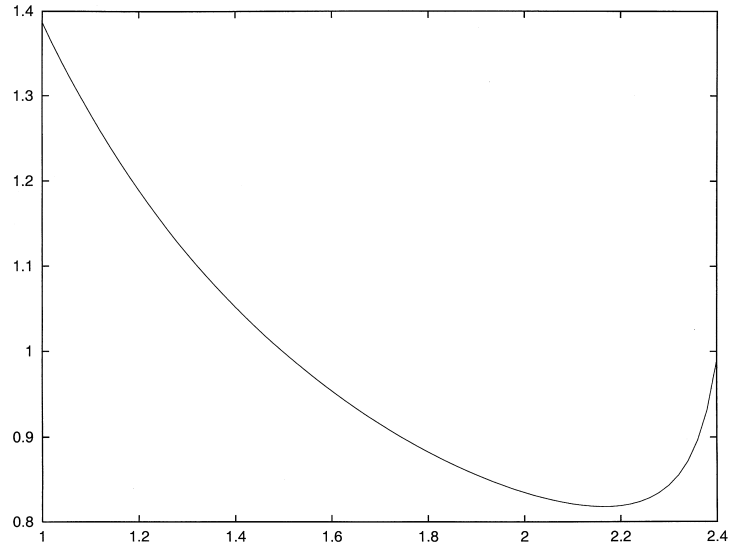

FIGURE 4. Values of F predicted by (22) as a function of k for $\kappa = 0.4$ and $1 < k < 2.4$.

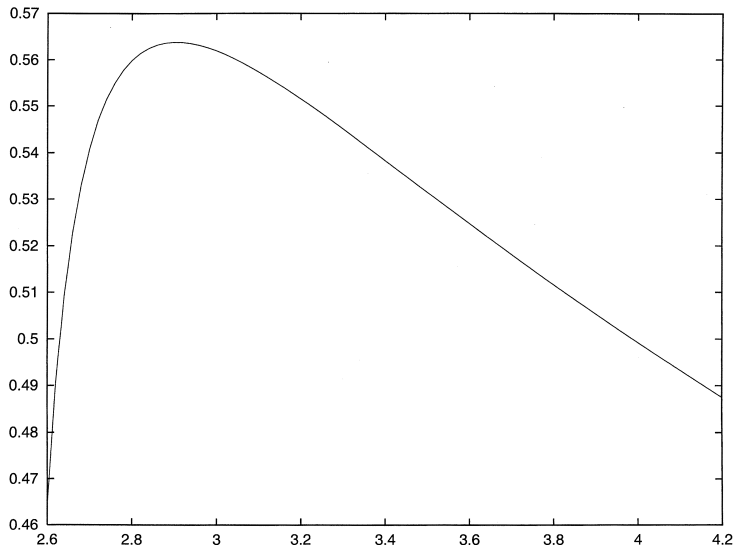

FIGURE 5. Same as Figure 4 for $2.6 < k < 4.2$.

Values of F^2 for $\kappa = 0.4$ and two different ranges of values of k are shown in Figures 4 and 5. From Figure 4, we see that there are two values $k_1 = 2.36$ and $k_2 = 1.76$ of k corresponding to the value $F = 0.89$ of Figure 2. Then k_1 satisfies (25) and k_2 satisfies (26). This explains why the waves of shorter wavelength are at the front of the distribution of pressure in Figure 2. We note that since Figure 2 corresponds to $R = 60$ instead of $R = \infty$, $k_1 = 2.36$ is not equal to $k_r^{front} = 2.94$ and $k_2 = 1.76$ is not equal to $k_r^{back} = 1.07$. However, the differences between these values decrease as R increases.

From Figure 5, we see that there are two values $k_1 = 3.26$ and $k_2 = 2.72$ corresponding to the value $F = 0.55$ of Figure 3. But now k_1 satisfies (26) and k_2 satisfies (25). Therefore, the waves of shorter wavelength are now on the back.

https://doi.org/10.1017/S095679250100451X Published online by Cambridge University Press

The presence of a minimum in the dispersion relation (see Figure 4) is familiar in the classical theory of gravity capillary waves mentioned in the introduction. The presence of a maximum is more unusual and leads to the unexpected effect that the waves of short wavelength are at the back of the disturbance.

Our comparison between the analytical results (20) and the nonlinear numerical results in Figures 2 and 3 was restricted to ϵ small and to R large. The limit $R \to 0$ is also interesting. For $R = 0$ the surface of the dissipative layer is flat and the effect of surface tension vanishes. The problem reduces then to the one considered by Vanden-Broeck & Miloh [9]. There is then only one train of waves at the back of the distribution of pressure. The results of [9] shows the inclusion of a dissipative layer (i.e. solving the problem with R small) fixes uniquely the solution. In other words, a dissipative layer is an alternative to the Rayleigh viscosity discussed in the introduction.

Finally, let us mention that the effect of increasing ϵ was studied in [9] for the particular case $T = 0$.

4 Conclusions

We have used a boundary integral equation method to calculate the free surface flow due to a moving distribution of pressure when the bottom is covered by a dissipative layer (modelled by the lubrication equations). The solutions were found to depend upon six parameters F, κ, R, δ, β, b and ϵ. We have calculated solutions with trains of waves on the free surface and demonstrated that the short train of waves does not always occur in front of the distribution of pressure. This numerical finding was clarified by examining analytically the asymptotic behaviour of the flow in the far field.

References

[1] Forbes, L. K. & Schwartz, L. W. (1982) Free-surface flow over a semicircular obstruction. *J. Fluid Mech.* **114**, 299–314.
[2] Lamb, H. (1932) *Hydrodynamics, 6th ed.* Cambridge University Press.
[3] Lighthill, J. (1978) *Waves in Fluids, 1st ed.* Cambridge University Press.
[4] Milewski, P. A. & Vanden-Broeck, J.-M. (1999) Time dependent gravity–capillary flows past an obstacle. *Wave Motion*, **29**, 63–79.
[5] Miloh, T., Spivak, B. & Vanden-Broeck, J.-M. (2001). *Euro J. Mech. B/Fluids*. Submitted.
[6] Lord Rayleigh (1883) The form of standing waves on the surface of running water. *Proc. Lond. Math. Soc.* **15**, 69–78.
[7] Ruvinsky, K. D., Feldstein, F. I. & Freidman, G. I. (1991) Numerical simulations of the quasi-stationary stage of ripple excitation by steep–capillary waves. *J. Fluid Mech.* **230**, 339–353.
[8] Vanden-Broeck, J.-M. & Dias, F. (1992) Solitary waves in water of infinite depth and related free surface flows. *J. Fluid Mech.* **240**, 549–557.
[9] Vanden-Broeck, J.-M. & Miloh, T. (1996) The influence of a layer of mud on the train of waves generated by a moving pressure distribution. *J. Eng. Math.* **30**, 387–400.
[10] Vanden-Broeck, J.-M. & Tuck, E. O. (1977) Computation of near-bow or stern flows, using series expansion in the Froude number. *Proc. 2nd Int. Conf. on Numerical Ship Hydrodynamics*, Berkeley, CA.